1.3 The metallic state

When a large number of rare earth atoms are assembled to form a solid, the $4f$ electrons generally remain localized, in a sense which will be made more precise later, so that their magnetic properties closely resemble those in the free atoms. The external $5d$ and $6s$ electrons, on the other hand, become delocalized into *Bloch states*, extending throughout the metal and constituting the conduction-electron gas. The conduction electrons themselves make only a modest contribution to the magnetic moment, but by mediating the magnetic interactions they play a crucial role in determining the characteristic magnetic properties in the solid state. An understanding of the magnetism therefore requires a detailed description of the conduction electron gas, and this section is concerned with our theoretical and experimental knowledge of the Bloch states, and their influence on the structural properties of the metals. Some of these structural properties of the rare earth metals are collected in Table 1.2, from which it may be seen that the room-temperature structures are all close-packed, with a coordination number of 12, with the exception of Eu, which is bcc. The remaining elements all form hexagonal phases,

Table 1.2. Structural properties of the lanthanides.

Element	Structure (300 K)	Lattice const. a (Å)	c (Å)	Atomic rad. S (a.u.)	Density (g/cm^3)	Melt. point (K)
La	dhcp	3.774	12.171	3.92	6.146	1191
Ce(β)	dhcp	3.681	11.857	3.83	6.689	1071
Ce(γ)	fcc	5.161		3.81	6.770	
Ce(α)	fcc	4.85 (77 K)		3.58	8.16	
Pr	dhcp	3.672	11.833	3.82	6.773	1204
Nd	dhcp	3.658	11.797	3.80	7.008	1294
Pm	dhcp	3.65	11.65	3.78	7.264	1315
Sm	rhom	3.629	26.207	3.77	7.520	1347
Eu	bcc	4.583		4.26	5.244	1095
Gd	hcp	3.634	5.781	3.76	7.901	1586
Tb	hcp	3.606	5.697	3.72	8.230	1629
Dy	hcp	3.592	5.650	3.70	8.551	1687
Ho	hcp	3.578	5.618	3.69	8.795	1747
Er	hcp	3.559	5.585	3.67	9.066	1802
Tm	hcp	3.538	5.554	3.65	9.321	1818
Yb	fcc	5.485		4.05	6.966	1092
Lu	hcp	3.505	5.549	3.62	9.841	1936

although the hcp allotrope of Yb is only stable at low temperatures, and Ce has two separate fcc phases in addition to its dhcp form.

The heavy rare earths are all hcp, while the dhcp structure predominates among the lighter metals. These structures may be produced by stacking close-packed layers in the sequences ABAB and ABAC respectively, as shown in Fig. 1.3. The fcc structure corresponds to the stacking sequence ABCABC, while the Sm structure is ABABCBCAC. The latter has rhombohedral symmetry but it is frequently more convenient to consider it as hexagonal. The crystallographic a-axis is taken along the direction joining a pair of nearest neighbours in the hexagonal plane, the c-axis is normal to the plane, and the b-axis is orthogonal to the other two. The local, i.e. nearest-neighbour, symmetry in the fcc and hcp structure is, of course, cubic and hexagonal respectively. The dhcp structure, on the other hand, has two types of site and, for an 'ideal' $c/2a$ ratio of 1.633, their *local* symmetry alternates between cubic and hexagonal in the sequence chch, while the Sm structure corresponds to chhchh. As may be seen from Table 1.2, however, the $c/2a$ ratio is consistently smaller than the ideal value, so the 'cubic' sites have only approximate local cubic symmetry.

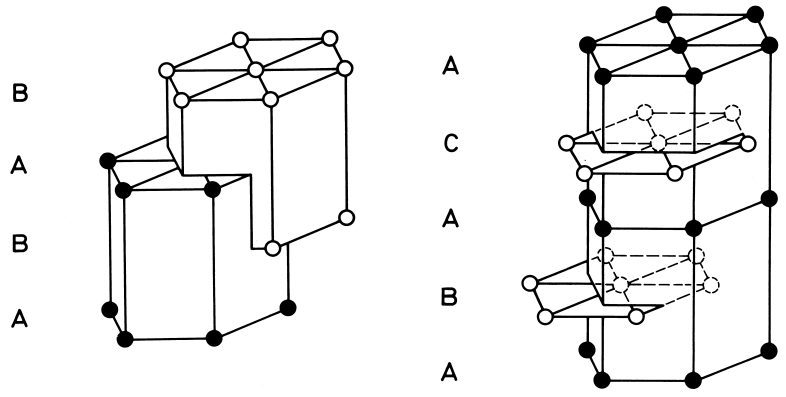

Fig. 1.3. The hcp and dhcp crystal structures. In the latter, the B and C sites have hexagonal symmetry, while the A sites have local cubic symmetry, for an ideal c/a ratio.

To determine the eigenstates for the conduction electron gas, we adopt the same procedure as that outlined for atoms in the previous section. The external potential $v_{\rm ext}(\mathbf{r})$ in (1.2.2) is now the Coulomb attraction of the nuclei situated on the crystal lattice, shielded by the electrons of the ionic core, which are usually taken to have the same charge distribution as in the atoms. The potential consequently has the translational symmetry of the periodic lattice, and so therefore does the effective potential $v_{\rm eff}(\mathbf{r})$, which arises when we make the single-particle approximation (1.2.5) and the local-density approximation (1.2.9). In the atom, the eigenfunctions are determined by the boundary condition that their amplitude must vanish for large values of r and, when (1.2.12) is integrated numerically, they are automatically continuous and differentiable. The translational symmetry of the solid is expressed in *Bloch's theorem*:

$$\psi(\mathbf{r}) = e^{i\mathbf{k}\cdot\mathbf{R}}\,\psi(\mathbf{r}-\mathbf{R}), \tag{1.3.1}$$

and this boundary condition gives rise to eigenfunctions $\psi_j(\mathbf{k},\varepsilon,\mathbf{r})$ and eigenvalues $\varepsilon_j(\mathbf{k})$ which are functions of the wave-vector $\mathbf{k}$ in reciprocal space. All the electron states may be characterized by values of $\mathbf{k}$ lying within the *Brillouin zone*, illustrated for the hexagonal and fcc structures in Fig. 1.4, and by the band index j defined such that $\varepsilon_j(\mathbf{k}) \le \varepsilon_{j+1}(\mathbf{k})$.

The determination of the eigenstates of the Schrödinger equation, subject to the Bloch condition (1.3.1) is the central problem of energy-band theory. It may be solved in a variety of ways, but by far the most

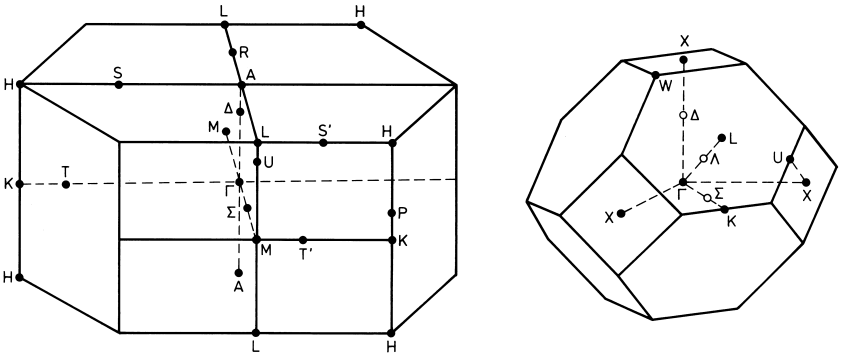

Fig. 1.4. The Brillouin zones for the hexagonal and fcc lattices.

effective procedure for the rare earths is to adopt one of the linear methods of Andersen (1975). In the following, we will use the *Atomic Sphere Approximation* (ASA) which will allow us to illustrate the construction and characteristics of the energy bands in a transparent way. This approximation, and the closely-related *Linear Muffin-Tin Orbitals Method* (LMTO), which allows computationally very efficient calculations of arbitrarily precise energy bands, for a given potential, have been concisely described by Mackintosh and Andersen (1980) and, in much more detail, by Skriver (1984).

In a close-packed solid, the electrons may to a very good approximation be assumed to move in a *muffin-tin potential*, which is spherically symmetric in a sphere surrounding each atomic site, and constant in the interstitial regions. We recall that the *atomic polyhedron*, or *Wigner–Seitz cell*, is bounded by the planes which perpendicularly bisect the vectors joining an atom at the origin with its neighbours, and has the same volume as the *atomic sphere*, whose radius S is chosen accordingly. If we surround each site in the crystal with an atomic sphere, the potential within each of these overlapping regions will, to a high degree of accuracy, be spherically symmetric. Neglecting the spin, we may therefore write the solutions of the Schrödinger equation for a single atomic sphere situated at the origin in the form

$$\psi_{lm}(\varepsilon, \mathbf{r}) = i^l R_l(\varepsilon, r) Y_{lm}(\hat{\mathbf{r}}), \tag{1.3.2}$$

where the radial function $R_l(\varepsilon, r)$ satisfies eqn (1.2.12) and is a function of the continuous energy variable ε. Examples of such radial functions are shown in Fig. 1.5.

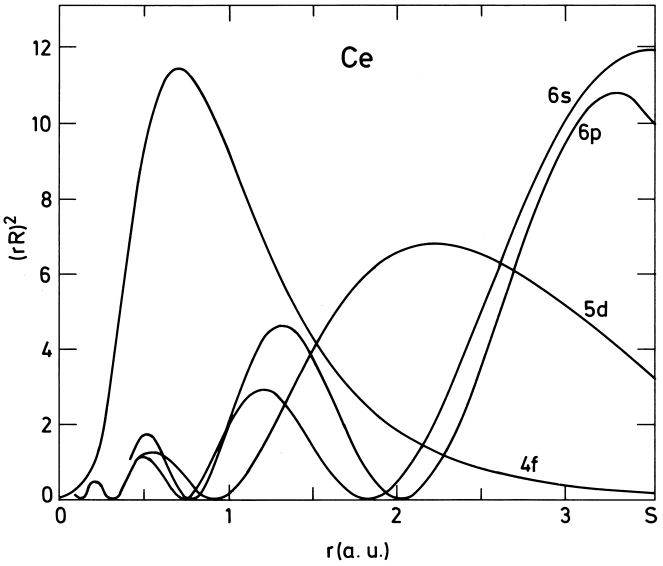

Fig. 1.5. Radial wavefunctions for α–Ce metal, calculated by Skriver from the self-consistent atomic-sphere potential, at the energies C_{nl} of the centres of the associated bands. Since these wavefunctions are normalized within the unit cell, the effective masses μ_{nl} are inversely proportional to the value of $R_l^2(C_{nl}, S)$ at the Wigner–Seitz radius, and this probability, and the consequent overlap between wavefunctions on neighbouring sites, therefore determines the corresponding band width.

Augmenting these partial waves by suitably-chosen regular solutions of Laplace's equation, we define the energy-dependent *muffin-tin orbitals*

$$\chi_{lm}(\varepsilon, \mathbf{r}) = i^l Y_{lm}(\hat{\mathbf{r}}) \begin{cases} R_l(\varepsilon, r) + p_l(\varepsilon)(r/S)^l \ ; & r < S \\ (S/r)^{l+1} \qquad\qquad\quad ; & r > S, \end{cases} \tag{1.3.3}$$

which are continuous and differentiable if

$$p_l(\varepsilon) = \frac{D_l(\varepsilon) + l + 1}{D_l(\varepsilon) - l}, \tag{1.3.4}$$

where the *logarithmic derivative* is

$$D_l(\varepsilon) = S\frac{R_l'(\varepsilon, S)}{R_l(\varepsilon, S)}. \tag{1.3.5}$$

From muffin-tin orbitals located on the lattice sites of a solid, with one atom per unit cell, we now construct a wavefunction which is continuous and differentiable, and manifestly satisfies the Bloch condition (1.3.1):

$$\psi_j(\mathbf{k},\varepsilon,\mathbf{r}) = \sum_{lm} a_{lm}^{j\mathbf{k}} \sum_{\mathbf{R}} e^{i\mathbf{k}\cdot\mathbf{R}} \chi_{lm}(\varepsilon, \mathbf{r}-\mathbf{R}). \tag{1.3.6}$$

If we approximate the atomic polyhedra by spheres, and implicitly assume that they fill space, the condition that (1.3.6) is a solution of the Schrödinger equation is easily seen to be that the sum of the tails originating from terms of the form $(S/|\mathbf{r}-\mathbf{R}|)^{l+1}$, from the surrounding atoms, cancels the 'extra' contribution

$$\sum_{lm} a_{lm}^{j\mathbf{k}} Y_{lm}(\hat{\mathbf{r}}) p_l(\varepsilon)(r/S)^l,$$

in the atomic sphere at the origin. To satisfy this condition, we expand the tails of the muffin-tin orbitals centred at $\mathbf{R}$ about the origin, in the form

$$\begin{aligned} \sum_{\mathbf{R}\neq\mathbf{0}} e^{i\mathbf{k}\cdot\mathbf{R}} \Big(\frac{S}{|\mathbf{r}-\mathbf{R}|}\Big)^{l+1} i^l Y_{lm}(\widehat{\mathbf{r}-\mathbf{R}}) \\ = \sum_{l'm'} \frac{-1}{2(2l'+1)} \big(\frac{r}{S}\big)^{l'} i^{l'} Y_{l'm'}(\hat{\mathbf{r}}) \mathcal{S}^{\mathbf{k}}_{l'm',lm}, \end{aligned} \tag{1.3.7}$$

where the expansion coefficients, known as the *canonical structure constants*, are

$$\mathcal{S}^{\mathbf{k}}_{l'm',lm} = \sum_{\mathbf{R}\neq\mathbf{0}} e^{i\mathbf{k}\cdot\mathbf{R}} \mathcal{S}_{l'm',lm}(\mathbf{R}), \tag{1.3.8}$$

with

$$\mathcal{S}_{l'm',lm}(\mathbf{R}) = g_{l'm',lm}\sqrt{4\pi}(-i)^{\lambda} Y^*_{\lambda\mu}(\hat{\mathbf{R}})(R/S)^{-\lambda-1},$$

where

$$g_{l'm',lm} \equiv (-1)^{m+1} 2 \sqrt{\frac{(2l'+1)(2l+1)}{2\lambda+1} \frac{(\lambda+\mu)!(\lambda-\mu)!}{(l'+m')!(l'-m')!(l+m)!(l-m)!}}$$

and

$$\lambda \equiv l + l' \;\; ; \;\; \mu \equiv m - m'.$$

From (1.3.3) and (1.3.7), the required *tail-cancellation* occurs if

$$\sum_{lm} [P_l(\varepsilon)\delta_{l'l}\delta_{m'm} - \mathcal{S}^{\mathbf{k}}_{l'm',lm}] a_{lm}^{j\mathbf{k}} = 0, \tag{1.3.9}$$

where the *potential function* $P_l(\varepsilon)$ is defined by

$$P_l(\varepsilon) = 2(2l+1)p_l(\varepsilon) = 2(2l+1)\frac{D_l(\varepsilon)+l+1}{D_l(\varepsilon)-l}. \tag{1.3.10}$$

The linear homogeneous equations (1.3.10) have solutions for the eigenvectors $a_{lm}^{j\mathbf{k}}$ only for those values of $\mathbf{k}$ and ε for which

$$\det\left[P_l(\varepsilon)\delta_{l'l}\delta_{m'm} - \mathcal{S}^{\mathbf{k}}_{l'm',lm}\right] = 0. \tag{1.3.11}$$

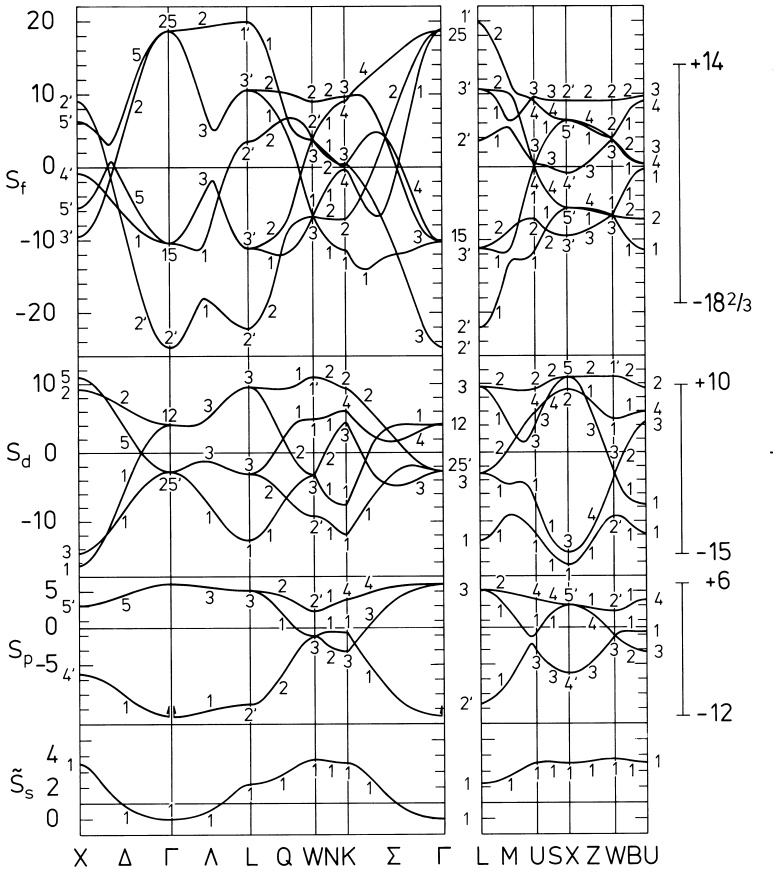

Fig. 1.6. The canonical bands for the fcc structure. The band structure in the metal may be obtained by placing, scaling, and distorting the canonical bands according to the values of the corresponding potential parameters C_{nl}, μ_{nl}, and γ_{nl}, and finally hybridizing them. The extent of the bands, according to the Wigner–Seitz rule, is indicated on the right.

In this determinantal equation for the band structure $\varepsilon_j(\mathbf{k})$, the information about the structure is separated from that on the potential. The structure constants $\mathcal{S}^{\mathbf{k}}_{l'm',lm}$ are canonical in the sense that they depend only on the crystal structure and not, for example, on the lattice constant, as may be seen from the definition (1.3.8), and the potential function $P_l(\varepsilon)$ is determined entirely by the potential within the atomic sphere. We shall consider these two terms in turn.

If we include values of l up to 3, i.e. s, p, d, and f partial waves, the structure constants form a square matrix with 16 rows and columns. The terms with $l = l'$ fall into 4 blocks, and these submatrices may be diagonalized by a unitary transformation from the lm to an lj representation. The $(2l+1)$ diagonal elements $\mathcal{S}^{\mathbf{k}}_{lj}$ of each sub-block are the unhybridized *canonical l bands*. The canonical bands for the fcc structure are shown in Fig. 1.6. If hybridization is neglected, which corresponds to setting to zero the elements of $\mathcal{S}^{\mathbf{k}}_{l'm',lm}$ with $l \neq l'$, eqn (1.3.11) takes the simple form

$$P_l(\varepsilon) = \mathcal{S}^{\mathbf{k}}_{lj}. \tag{1.3.12}$$

Since $P_l(\varepsilon)$ is a monotonically increasing function of energy, as illustrated in Fig. 1.7, the band energies $\varepsilon_{lj}(\mathbf{k})$ for the pure l bands are obtained by a monotonic scaling of the corresponding canonical bands. $P_l(\varepsilon)$ does not, furthermore, depart greatly from a straight line in the energy region over which a band is formed, so the canonical bands resemble the energy bands in the solid quite closely, whence the name.

The potential function $P_l(\varepsilon)$ and the logarithmic-derivative function $D_l(\varepsilon)$ are related to each other through the definition (1.3.10), and this relationship is shown schematically in Fig. 1.7. It is convenient and illuminating to parametrize the potential function, when considering the formation of the energy bands from the canonical bands. The poles of $P_l(\varepsilon)$, which occur when $D_l(\varepsilon) = l$, divide the energy into regions in which lie the corresponding atomic energy-levels ε_{nl}. The energies V_{nl} which separate these regions are defined by

$$D_l(V_{nl}) = l \tag{1.3.13}$$

and, within a particular region, the energy C_{nl} of the centre of the band is fixed by the condition that $P_l(C_{nl}) = 0$, or

$$D_l(C_{nl}) = -(l+1). \tag{1.3.14}$$

The allowed $\mathbf{k}$-values corresponding to this energy are just those for

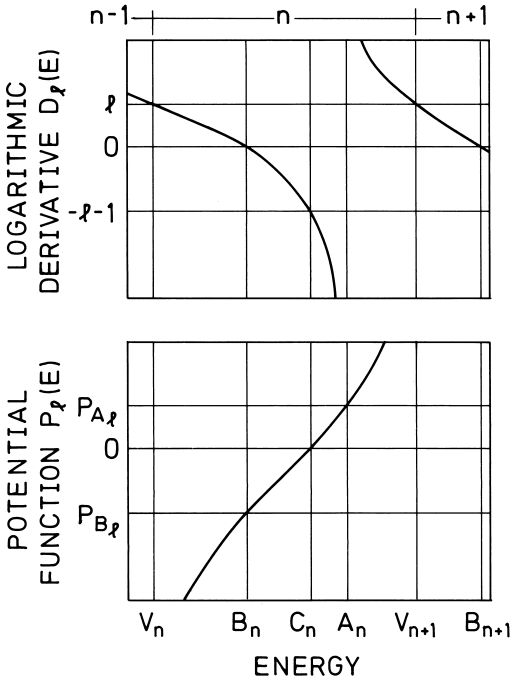

Fig. 1.7. The nth period of the logarithmic derivative function $D_l(\varepsilon)$, and the corresponding potential function $P_l(\varepsilon)$. The bottom, centre, and top of the nl band are defined respectively by $P_l(B_{nl}) = -2(2l+1)(l+1)/l$ $(D_l(B_{nl}) = 0)$, $P_l(C_{nl}) = 0$, and $P_l(A_{nl}) = l$ $(D_l(A_{nl}) = -\infty)$.

which $\mathcal{S}^{\mathbf{k}}_{lj} = 0$ and, since the average over the Brillouin zone may be shown to vanish, i.e.

$$\sum_{j=1}^{2l+1} \int_{BZ} \mathcal{S}^{\mathbf{k}}_{lj}\, d\mathbf{k} = 0, \tag{1.3.15}$$

the designation of C_{nl} as the centre of the band is appropriate. Equation (1.3.12) may be satisfied, and energy bands thereby formed, over an energy range around C_{nl} which, to a good approximation, is defined by the Wigner–Seitz rule, which states that, by analogy with molecular binding, the top and bottom of the band occur where the radial wavefunction and its derivative respectively are zero on the atomic sphere. The corresponding energies, defined by

$$D_l(A_{nl}) = -\infty \tag{1.3.16}$$

and

$$D_l(B_{nl}) = 0, \tag{1.3.17}$$

are then known respectively as the top and bottom of the nl band, even though this designation is not precisely accurate.

Over the energy range A_{nl}–B_{nl}, the potential function may be parametrized with reasonable accuracy as

$$P_l(\varepsilon) \simeq \frac{1}{\gamma_{nl}} \frac{\varepsilon - C_{nl}}{\varepsilon - V_{nl}}. \tag{1.3.18}$$

It is convenient to define the related mass parameter μ_{nl} by

$$\mu_{nl} S^2 = \left. \frac{dP_l(\varepsilon)}{d\varepsilon} \right|_{C_{nl}} \simeq \frac{1}{\gamma_{nl}(C_{nl} - V_{nl})}. \tag{1.3.19}$$

It is determined by the probability that an electron described by the partial wave $R_l(C_{nl}, r)$ reaches the atomic sphere and, if the wavefunction is normalized within the sphere, it may be shown that

$$\mu_{nl} S^2 = \left[\tfrac{1}{2} S R_l^2(C_{nl}, S) \right]^{-1}. \tag{1.3.20}$$

For free electrons, $\mu_{nl} \equiv 1$ for all values of n and l.

With this parametrization, we may write down an explicit expression for the unhybridized band energies. From eqns (1.3.12), (1.3.18) and (1.3.19) these are given by

$$\varepsilon_{lj}(\mathbf{k}) = C_{nl} + \frac{1}{\mu_{nl} S^2} \frac{\mathcal{S}_{lj}^{\mathbf{k}}}{1 - \gamma_{nl} \mathcal{S}_{lj}^{\mathbf{k}}}. \tag{1.3.21}$$

The pure l bands are thus obtained from the corresponding canonical bands by fixing the position with C_{nl}, scaling the bandwidth by $\mu_{nl} S^2$, and distorting them with γ_{nl}.

Hybridization between bands of different l is taken into account by including the structure constants with $l \neq l'$ in (1.3.11), causing a repulsion between energy levels with the same $\mathbf{k}$ and symmetry, as specified by the labels in Fig. 1.6. Bands of the same symmetry are thus not allowed to cross, and *strong hybridization* instead creates an energy gap. In addition, *weak hybridization* gives rise to a mixing and repulsion between bands which do not cross in the absence of hybridization. In order to complete the calculation of the band structure, the inaccuracies due to approximating the atomic polyhedron by a sphere, and to neglecting higher partial waves, may be conveniently treated together by perturbation theory. In practice, the energy bands are not of course calculated step-wise as described above, but all the steps are performed simultaneously on a computer. Nevertheless, the conceptual description of the procedure as a placing, scaling and distortion of the

canonical bands, according to the values of the potential parameters, with a final hybridization between bands of the same symmetry, allows a clear visualization of the way in which the relatively complex band structure is built up from simpler elements, and of the relation between the eigenstates of the atom and those in the solid.

Table 1.3. Electronic parameters for α–Ce.

	$6s$	$6p$	$5d$	$4f$
A_l (Ry)	2.234	2.698	1.198	0.648
C_l (Ry)	0.620	1.452	0.792	0.628
B_l (Ry)	0.330	0.909	0.409	0.587
μ_l	0.61	0.70	2.18	45.36
n_l	0.509	0.245	2.091	1.154
$N_l(\varepsilon_F)$ (Ry^{-1})	1.81	1.50	6.48	21.11
$\mathcal{P}_l\Omega$ (Ry)	0.195	0.152	−0.219	−0.163

This procedure may be illustrated by considering the construction of the band structure of α–Ce from its component parts. Partial waves in the atomic sphere at the energies of the band-centres, where $P_l(\varepsilon) = 0$, are shown in Fig. 1.5, and the corresponding potential parameters are given in Table 1.3. In this section, we express the energies in Rydbergs, following our general principle of using throughout the book those units which are favoured by practitioners of research in the subject currently under discussion. The s and p effective masses are somewhat below 1, and the relative positions of the band centres correspond quite closely to those of the free-electron gas. Through the influence of the l-dependent centrifugal-potential term in (1.2.12), the d and f states are in contrast constrained to the inner regions of the atomic sphere, with the consequence that the d mass is relatively large (though not as large as in a typical transition metal) and the f mass is extremely large.

The energy bands of Fig. 1.8 were calculated by an iterative procedure, by Skriver (private communication). The electron density $n(\mathbf{r})$ is first estimated by, for example, overlapping *atomic* charge densities situated on the lattice sites, and from it the periodic potential $v_{\mathrm{eff}}(\mathbf{r})$ is constructed, using the local-density approximation (1.2.9). The band structure is then determined for this potential and $n(\mathbf{r})$ recalculated, in analogy with (1.2.6), by summing over occupied states, those beneath the Fermi level. This procedure is repeated until the potential self-consistently reproduces itself, and the energy bands have converged to the desired accuracy. The band structure can be considered as being

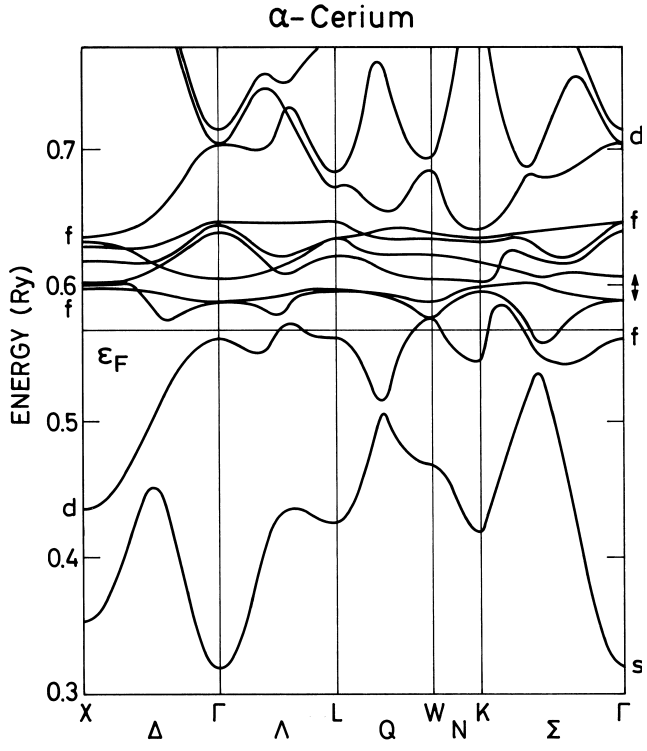

Fig. 1.8. The band structure of fcc α–Ce, calculated by Skriver. The orbital angular momentum of some states at symmetry points in the zone is indicated, including the top and bottom of the narrow bands. The doubleheaded arrow indicates the spin–orbit splitting of a $4f$ state.

composed of a broad free-electron-like *sp* band, crossed by and hybridizing both strongly and weakly with the d and f bands. The occupation numbers n_l of the various states given in Table 1.3 make it clear that α–Ce may be classified as both a d- and an f-band transition metal.

The above description of the f states in α–Ce as occupying the bottom of an f band is now generally accepted as valid, but the correct treatment of the f electrons in the rare earth metals, and especially Ce, was a matter of lengthy controversy. According to the standard model, which is generally applicable to rare earth magnetism, an integral number of f electrons are localized on each ion, subject to the same intra-ionic interactions as in the free atom. The Pauling–Zachariasen promotional model for the γ–α phase transition in Ce, which associated the transition with the transfer of a single f electron on each ion to a d state, with a concomitant decrease of about 6% in the fcc lattice

constant, was therefore consistent with the standard model. However the positron-annihilation experiments of Gustafson and Mackintosh (1964) showed that the change in f occupancy, when the transition was induced by a change in temperature, was much less than one, and indeed that the results in both phases were consistent with about one f electron per ion. Similar results were obtained by Gustafson *et al.* (1969) when the transition was driven by pressure, and they concluded that it involves not primarily a change in the f *occupancy* but rather a change in the f *state*, from being localized in the γ-phase to being an itinerant band electron in the α-phase. This idea was taken up by Johansson (1974) who, from a consideration of spectroscopic, cohesive and thermodynamic evidence, proposed that the γ–α transition should be considered as a Mott localized–delocalized transition among the f electrons. Glötzel (1978) used density-functional theory to calculate the ground state properties and showed that the equation of state in the α-phase can be accounted for rather satisfactorily by including the f electrons in the band structure, and furthermore that a transition to a spin-polarized state should occur at a lattice constant close to that of γ–Ce, though at a (negative) pressure considerably lower than that deduced from experiment. Eriksson *et al.* (1990) have recently shown that this discrepancy may be substantially reduced by including the l–l coupling, which is responsible for the second of Hund's rules, in the calculation of the $4f$ bands. This leads to a ground state in γ–Ce in which the $4f$ electrons are almost fully polarized, thus occupying the Hund's-rule ground state on each site. Despite the fact that they are described in the band picture, they may thus be considered as *localized*, making very little contribution to the cohesive properties. The calculated atomic volumes in both phases are in good agreement with experiment. Podloucky and Glötzel (1983) found a cohesive energy for α–Ce in accord with the measured value, while that of a 'promotional' state with no f electrons is far too small. They were also able to account for the Compton-scattering experiments of Kornstädt *et al.* (1980), who had verified that the change in f occupancy at the transition is small. Skriver (1985) calculated the crystal structure and equation of state of α–Ce up to high pressures, finding very good agreement with experiment (Staun Olsen *et al.* 1985), provided that the f bands are included, but very poor agreement if the f electrons are promoted to the d bands, or are assumed to be localized, and therefore to make a negligible contribution to the electronic pressure. The relative stability at high pressures of low-symmetry configurations such as the α–U structure, which is observed experimentally, is a strong indicator that there are f electrons in the conduction bands, as in the light actinides, where they play a decisive role in determining the structure (Skriver 1985).

The most powerful experimental technique available for studying the details of the electronic structure in the vicinity of the Fermi level is the de Haas–van Alphen (dHvA) effect (Shoenberg 1983), which allows a precise determination not only of the shape of the Fermi surface, but also of the effective masses of the electrons whose wave-vectors lie on it. Unfortunately, the metallurgical difficulties encountered in attempting to fabricate pure single crystals have so far precluded the observation of the effect in α–Ce, but Johanson *et al.* (1981) studied the related compound $CeSn_3$, and demonstrated that it contains itinerant f electrons of large mass at low temperatures. More recently, a number of examples of heavy-fermion Ce compounds have been investigated (Reinders *et al.* 1986; Lonzarich 1988) in which the effective masses, as deduced either from the dHvA effect or the low-temperature heat capacity, are enhanced by up to an order of magnitude compared with those deduced from band structure calculations.

There is thus very convincing evidence that the f electrons in Ce and its compounds can form bands and extend in coherent Bloch states throughout the crystal. Photoemission experiments in α–Ce (Wieliczca *et al.* 1982; Mårtensson *et al.* 1982) revealed a structure with two peaks, which may plausibly be associated respectively with an itinerant f hole near the Fermi level, and one localized for a finite time at a particular ionic site (Norman *et al.* 1984; Mackintosh 1985). There are very few indications of itinerant f behaviour in the other rare earth elements, although the above-mentioned double-peaked structure is also observed in γ–Ce and Pr (Wieliczka *et al.* 1984), in both of which the f electrons are normally considered as localized, and as we shall see, there is evidence of an f contribution to the binding energy in some of the light rare earths. After this brief interlude, we will therefore leave the question of f bands and return to the standard model of f electrons localized on the ions, interacting with the surroundings but only indirectly with each other.

Pr, the neighbouring element to Ce, undergoes a phase transition at high pressures (Wittig 1980) which is probably associated with the formation of a band by the f electrons (Skriver 1981; Eriksson *et al.* 1990), but at ambient pressures they are localized and may be considered as part of the ionic core. Indeed, intermultiplet transitions, corresponding to those occurring on Pr ions in insulators, but shifted due to screening by the conduction electrons in the metal, have been observed by Taylor *et al.* (1988), using inelastic neutron-scattering at relatively high energies. The $4f$ states do not therefore appear in the energy bands of Fig. 1.9, which portrays broad *sp* bands hybridized with a much narrower d band. As will be discussed later, Pr is paramagnetic above about 50 mK, and in zero field the Fermi surface, which is relatively complex, may be deduced from the figure to be composed of 2 electron pockets and 4 open

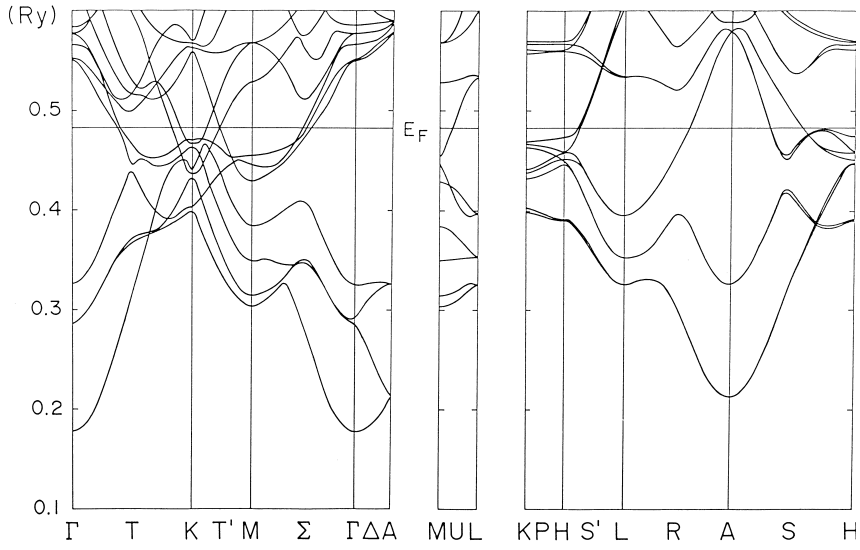

Fig. 1.9. The band structure of dhcp Pr, calculated by Skriver. The energy bands in the vicinity of the Fermi level are predominantly d-like, and the $4f$ states are assumed to be localized and therefore do not appear, in contrast to Fig. 1.8.

hole sheets. However, the dHvA effect is measured in a relatively high magnetic field, and the induced moment modifies the band structure in a way which has been studied in detail by Wulff (1985). The exchange coupling between a conduction-electron spin $\mathbf{s}$ and the $4f$ spins takes the Heisenberg form

$$\mathcal{H}_{\rm sf} = -2I\mathbf{s}\cdot\sum_i \mathbf{S}_i. \tag{1.3.22}$$

In the ground-state manifold, this interaction may from (1.2.29) be written

$$\mathcal{H}_{\rm sf} = -2(g-1)I\mathbf{s}\cdot\sum_i \mathbf{J}_i. \tag{1.3.23}$$

When a magnetic field is applied, the induced moment therefore gives rise to a splitting between the up- and down-spin energy bands. Since Pr is magnetically highly anisotropic, this splitting depends strongly on the direction of the field, but it can readily attain values of several mRy, and hence have drastic effect on the Fermi surface. In particular, the seventh-band minority-spin surface changes its topology at a critical (internal) field of about 40 kOe, as shown in Fig. 1.10,

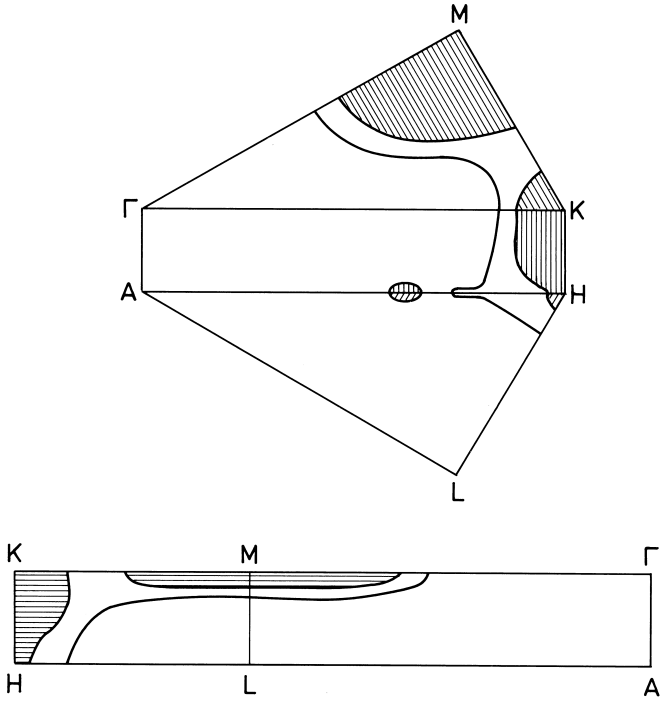

Fig. 1.10. The intersections of the Fermi surfaces, for the two spin states of the seventh band in dhcp Pr, with the faces of the Brillouin zone of Fig. 1.4. The surfaces are generated by a rigid splitting of the energy bands of Fig. 1.9 by 10 mRy. The unshaded majority-spin surface is a single sheet, whereas the exchange splitting modifies the topology of the shaded minority-spin surface, giving rise to a closed lens at M, a small electron pocket, and an irregular tube along HK.

and clear evidence for this transition has been observed in the dHvA effect. The changes of the Fermi surface in a magnetic field, and particularly the enhancement of the effective masses by the interaction with the $4f$ moments (Wulff *et al.* 1988), which we will discuss further in Section 7.3, give an average value of I of about 9 mRy, with a variation of some 30% over different bands and orbits. The agreement between the measured and calculated electron orbits is such that shifts in the energy bands of only a few mRy are required to bring the two into concordance, and this is comparable to typical values for transition metals (Mackintosh and Andersen 1980). The experimental study of the dHvA effect in Pr, which is the most elaborate which has yet been undertaken for a rare earth metal, has thus led to the important conclusion that energy-band

theory gives a realistic description of the conduction electron states, and may therefore be used as a basis for the calculation of properties which depend on the electronic structure.

This conclusion could already be drawn, though with slightly less confidence, from the pioneering measurements of Mattocks and Young (1977) of the dHvA effect in ferromagnetic Gd. Because of the ferromagnetic moment, the exchange interaction (1.3.22) separates the energy bands of different spin even in zero field, and the exchange splitting is essentially independent of field. The results were interpreted in terms of the paramagnetic energy bands, originally calculated by Dimmock and Freeman (1964) and, with relativistic effects, by Keeton and Loucks (1968), taking account of the ferromagnetic structure by a rigid splitting of the bands. The resulting two majority-spin hole surfaces and the minority-spin electron surface could account for all of the observed large orbits, with a value of I close to that later deduced for Pr, and with a comparable variation through the zone. However, many small orbits were observed which could not be explained with this model, nor have subsequent band calculations, culminating in those of Temmerman and Sterne (1990), in which the exchange splitting of the conduction bands was included a priori, fully accounted for the small pieces of the Fermi surface. Although the general features of the electronic structure of Gd may therefore be considered as well understood, a further theoretical effort, taking into account the effect on the band structure of the spin–orbit coupling in the presence of both an exchange field and an external field, would be necessary to explain the finer details.

The positron-annihilation experiments of Williams and Mackintosh (1968), although at a much lower level of resolution, were also in general accord with the calculations of Keeton and Loucks (1968). They studied a number of heavy rare earths in their paramagnetic phases, showing that their Fermi surfaces are highly anisotropic and rather similar to each other. A calculation based upon energy-band theory gave a good account of the experimental results for Y. The distributions of the annihilation photons displayed a feature which is sensitive to the form of the hole surface shown in Fig. 1.11, namely the shape of the 'webbing' which may join the 'toes' on the surface near L. This characteristic is very dependent on the relative positions of the s and d bands, and the calculations indicated that the webbing is absent in Gd, very narrow in Tb, and fully developed, forming a kind of plateau, in the other heavy rare earths. These conclusions were in accordance with the positron-annihilation results, which further indicated that the webbing is destroyed in the magnetically ordered phase of Ho. The relation of these observations to the occurrence of periodic magnetic structures will be discussed in the following section.

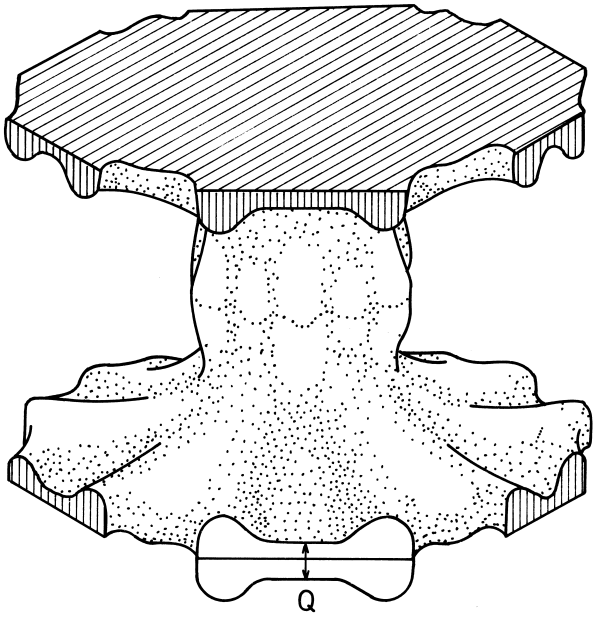

Fig. 1.11. The calculated hole Fermi surface of paramagnetic Tb in the Brillouin zone of Fig. 1.4. The extension of the 'webbing' between the 'toes' near the zone boundary is believed to give rise to a peak in the conduction-electron susceptibility $\chi(\mathbf{q})$, which determines the $\mathbf{Q}$-vector characterizing the helical structure.

The Fermi surface of paramagnetic Lu, in which the $4f$ states are all filled, has also been studied by the dHvA effect (Johanson *et al.* 1982) and found to be in semi-quantitative agreement with the calculations of Tibbetts and Harmon (1982). Since the results of band structure calculations have been confirmed experimentally at the Fermi level in widely separated elements in the rare earth series, it is reasonable to suppose that they will also be successful in accounting for other ground-state properties. Characteristic band energies for the trivalent lanthanides, calculated by Skriver (1983) at a common atomic volume close to the equilibrium value for Gd, are shown in Fig. 1.12. In this figure, the effect of the change in potential is thus separated from that of the interatomic spacing. The most notable feature is the fall in energy of the s band relative to the d band with increasing atomic number, which results in a decrease of the occupation of the latter, with consequences, as we shall

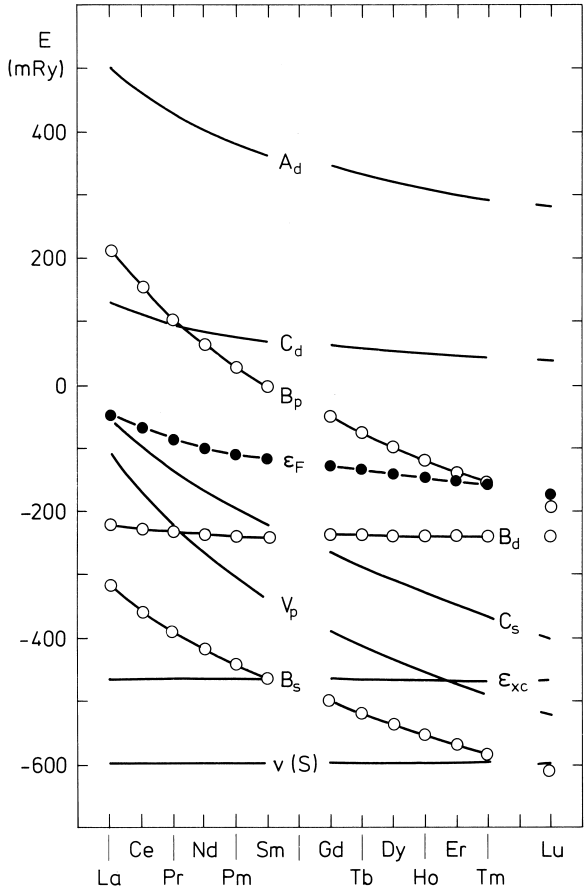

Fig. 1.12. Characteristic band energies for the trivalent lanthanides, for a common value of the atomic radius S, after Skriver (1983). The values of the potential *v(S)* and the exchange-correlation energy ε_{xc} at the atomic sphere are shown, together with the bottom, B_l, the centre, C_l, and the top, A_l, of the $6s$, $6p$, and $5d$ bands, and the Fermi level ε_F. The relative lowering of the $6s$ band with increasing atomic number reduces the $5d$ occupancy, which in turn changes the crystal structure.

see, for the crystal structure. The reason for the fall in the band energies is the increase of the nuclear charge with atomic number, which is incompletely screened by the additional f electrons. The potential $v_{\text{eff}}(\mathbf{r})$ in (1.2.12) is therefore on average increasingly negative, and in order to maintain an unchanged boundary condition, as expressed by the logarithmic derivative, the band energies must decrease accordingly.

This effect is relatively modest for the d bands, but much greater for the s and p bands. The relative shift of the s and d bands is reduced by the adjustment of the lattice to its equilibrium configuration, but only by a small amount. As may be seen from Fig. 1.12, $(B_d - B_s)$ increases from 101 mRy for La to 373 mRy for Lu at constant S, whereas the corresponding values for the equilibrium atomic volumes are 136 mRy and 380 mRy. The band masses also change across the series; μ_d at constant volume increases from 2.1 in La to 3.0 in Lu, so that the d bands narrow as they fall, while μ_s increases slightly with atomic number, but remains below 1 throughout (Skriver 1983).

The canonical-band theory may be used to calculate the electronic pressure and its partitioning between the different angular momentum components. According to the *force theorem* (see Mackintosh and Andersen 1980) the change in the total energy, due to an infinitesimal change in the lattice constant, may be determined as the difference in the band energies, calculated while maintaining the potential unchanged. We may thus write

$$dU = \delta \int^{\varepsilon_F} \varepsilon N(\varepsilon) d\varepsilon, \tag{1.3.24}$$

where $N(\varepsilon)$ is the total electronic density of states, and δ indicates the restricted variation with a *frozen potential*. The electronic pressure is then given by

$$\mathcal{P} = -\frac{dU}{d\Omega}, \tag{1.3.25}$$

where Ω is the volume of the atomic polyhedron. The expression (1.3.21) for the canonical-band energies then leads to the approximate result for the l partial pressure:

$$3\mathcal{P}_l\Omega = -n_l \frac{\delta C_l}{\delta \ln S} + n_l(\overline{\varepsilon}_l - C_l)\frac{\delta \ln \mu_l S^2}{\delta \ln S}, \tag{1.3.26}$$

where n_l is the occupation number of the l states and

$$\overline{\varepsilon}_l = \frac{1}{n_l}\int^{\varepsilon_F} \varepsilon N_l(\varepsilon) d\varepsilon \tag{1.3.27}$$

is their mean energy. Equation (1.3.26) is useful for purposes of interpretation, but the results which we shall present are based upon a more accurate procedure, involving the fully hybridized self-consistent band structure (Skriver 1983).

The partial occupation numbers, state-densities and electronic pressures for α–Ce, at the equilibrium lattice constant, are given in Table 1.3. The s and p electrons make a positive, repulsive contribution to

the pressure while the d and f states provide the binding, through their negative, attractive partial pressure. This difference is essentially due to the fact that the s and p wavefunctions have a positive curvature at the atomic sphere, over the energy range of the corresponding bands, as illustrated in Fig. 1.5, while the d and f functions have a negative curvature. Consequently, a decrease in volume causes an increase in the logarithmic derivative for the former and a decrease for the latter, and since $D_l(E)$ is a decreasing function of energy, the s and p bands must rise and the d and f bands fall in order to maintain the boundary condition. Equation (1.3.25) then immediately accounts for the signs of the corresponding partial pressures. The attractive f pressure for α–Ce is substantial; if it is removed, the lattice expands to a volume greater than that of γ–Ce. The partial pressures at a constant atomic volume for the trivalent rare earths are shown in Fig. 1.13. As may be seen, it is primarily the decrease in the s and p pressures, which has its origin in the incompletely

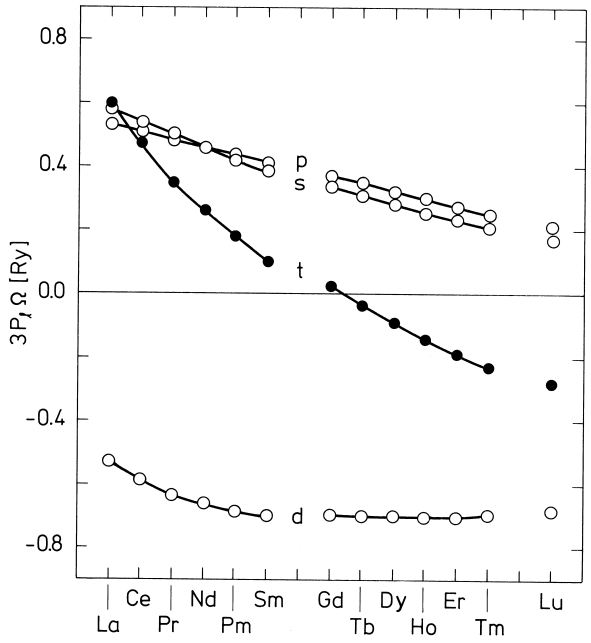

Fig. 1.13. The partial $6s$, $6p$, and $5d$ pressures for the trivalent rare earths, calculated for a common atomic volume close to the equilibrium value for Gd, after Skriver (1983). It is the decrease in the s and p pressures which gives rise to the lanthanide contraction.

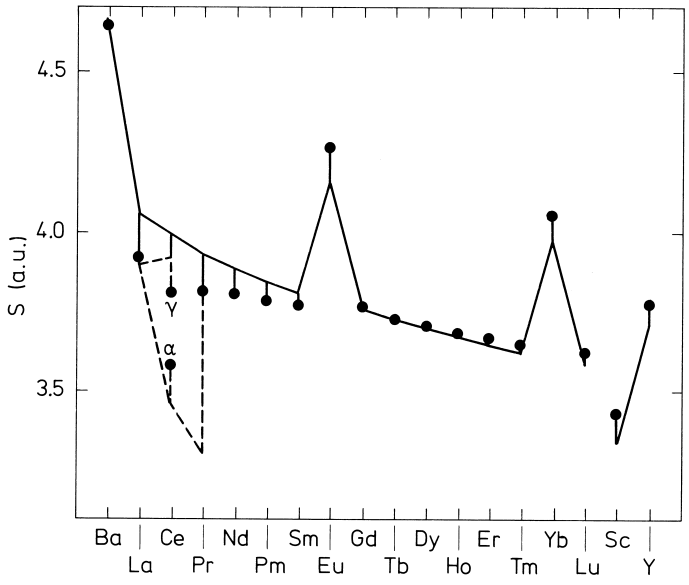

Fig. 1.14. The equilibrium atomic radii for the rare earth metals, after Skriver (1983). The full circles indicate the experimental values. The full line is a calculation including the s, p, and d partial pressures, while the broken line indicates that the f contribution is also taken into account.

screened increase in the nuclear charge, which leads to the lanthanide contraction. This contraction is clearly apparent in the atomic radii shown in Fig. 1.14. The values calculated from the condition that the total pressure is zero agree very well with the experimental observations for the heavy metals, but if the f contribution is neglected, the calculated electronic pressure is increasingly too high as the atomic number decreases. As mentioned earlier, the partial pressure of the f band is essential for understanding α–Ce, and it seems that the interaction of the f electrons with their surroundings makes a contribution to the binding, even in some metals in which the magnetic behaviour strongly indicates that they are localized.

In Eu and Yb, the intra-atomic interactions make it favourable to (half) fill the sub-band by transferring an electron from the conduction bands to an f state, leading to the formation of the divalent cubic structures which strongly resemble the alkaline earth metals. This transfer occurs predominantly at the expense of the d electrons, whose binding contribution to the electronic pressure is thereby reduced, causing

a substantial increase in the atomic volume. The relatively weak binding of the $4f$ states in the divalent rare earths is clearly apparent in the experiments of Lang *et al.* (1981), who used X-ray photoemission to measure the energies required to transfer a $4f$ electron to the Fermi level, throughout the whole series. By inverse photoemission *(Bremsstrahlung Isochromat Spectroscopy)* they were similarly able to deduce the energies required to move an electron from the Fermi level to the unoccupied $4f$ states. Combining the two experiments, the Coulomb correlation energy required to transfer an electron from an occupied level on another site could be deduced. These energies were later calculated by Min *et al.* (1986a) using a supercell method, in which rare earth ions with different f occupancies are considered as distinct species, and the agreement with experiment was generally very satisfactory.

For close-packed structures, the atomic volume is almost independent of the structure, but there are small differences in the electronic contribution to the cohesive energy, which manifest themselves in the common structural sequence hcp → dhcp → Sm-structure → fcc in the rare earths, as the atomic number is reduced or the pressure is increased. Duthie and Pettifor (1977) proposed that the d-electron occupancy,

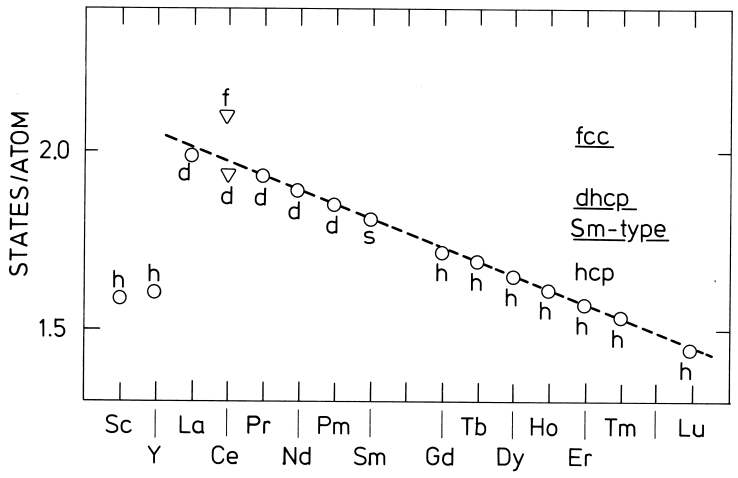

Fig. 1.15. The occupation numbers of the $5d$ states for the trivalent lanthanides, at the observed equilibrium atomic volumes, after Skriver (1983). For Ce, the $4f$ electrons are included in the energy bands. The experimentally observed crystal structures are labelled by h, s, d, and f, for hcp, Sm-structure, dhcp, and fcc, respectively. The empirical d-occupation numbers which separate the different structures are indicated by the lines on the right.

which increases through these structural sequences, is the essential determinant of the structure, and made an approximate calculation of the energy differences using canonical-band theory. The results of Skriver (1983) in Fig. 1.15 show how well the d occupancy indeed correlates with the structure. To complete the picture, Min *et al.* (1986b) demonstrated that increasing the pressure on Lu should produce a series of phase transitions following the above sequence, the first of which has been observed experimentally.